Published in final edited form as:
Cancer Res. 2009 April 1; 69(7): 3196–3204. doi:10.1158/0008-5472.CAN-08-3358.

CD47 Regulates Bone Mass and Tumor Metastasis to Bone

Özge Uluçkan[1], **Stephanie N. Becker**[1], **Hongju Deng**[1], **Wei Zou**[2], **Julie L. Prior**[3], **David Piwnica-Worms**[3], **William A. Frazier**[4], and **Katherine N. Weilbaecher**[1]

[1]Division of Oncology, Department of Medicine and Cell Biology and Physiology, Washington University School of Medicine, St. Louis, Missouri

[2]Department of Pathology and Immunology, Washington University School of Medicine, St. Louis, Missouri

[3]Molecular Imaging Center, Mallinckrodt Institute of Radiology, and Department of Molecular Biology and Pharmacology, Washington University School of Medicine, St. Louis, Missouri

[4]Department of Biochemistry and Molecular Biophysics, Washington University School of Medicine, St. Louis, Missouri

Abstract

CD47, also called integrin-associated protein, plays a critical role in the innate immune response and is an atypical member of the immunoglobulin superfamily that interacts with and activates β3 integrins. β3 integrin$^{-/-}$ mice have defective platelet and osteoclast function and are protected from bone metastasis. The role of CD47 in skeletal homeostasis and bone metastasis has not been described. CD47$^{-/-}$ mice had increased bone mass and defective osteoclast function *in vivo*. Although the number of functional osteoclasts formed by differentiating CD47$^{-/-}$ bone marrow macrophages was decreased, high doses of RANKL rescued differentiation and function of CD47$^{-/-}$ osteoclasts *ex vivo* and rescued the osteoclast defect in CD47$^{-/-}$ mice. Inhibition of nitric oxide (NO) synthase, which is expressed at higher levels in CD47$^{-/-}$ osteoclasts, also rescued the osteoclast defect in CD47$^{-/-}$ cells. We then examined the consequences of this osteoclast defect in bone metastasis. In a model of tumor metastasis to bone, bone tumor burden was decreased in the CD47$^{-/-}$ mice compared with wild-type (WT) controls, with no decrease in s.c. tumor growth in CD47$^{-/-}$ mice. There was decreased tumor-associated bone destruction in the CD47$^{-/-}$ mice compared with WT controls, consistent with a defect in osteoclast function that was not rescued by the presence of tumor. Our data show that CD47 regulates osteoclastogenesis, in part, via regulation of NO production, and its disruption leads to a decrease in tumor bone metastasis. CD47 is a novel therapeutic target to strengthen bone mass and diminish metastatic tumor growth in bone.

Introduction

Bone metastases cause hypercalcemia, bone loss, fractures, and pain and are thus a significant cause of morbidity and mortality in cancer patients (1). Several tumor cell types (e.g., breast and prostate carcinomas and melanomas) metastasize to bone and lead to bone degradation via

Requests for reprints: Katherine N. Weilbaecher, Division of Oncology, Department of Medicine and Cell Biology and Physiology, Washington University School of Medicine, 660 South Euclid, Box 8069, St. Louis, MO 63110. Phone: 314-454-8858; Fax: 314-454-8979; E-mail: kweilbae@im.wustl.edu.

Note: Supplementary data for this article are available at Cancer Research Online (http://cancerres.aacrjournals.org/).

Disclosure of Potential Conflicts of Interest
No potential conflicts of interest were disclosed.

activation of bone-resorbing osteoclasts (1–4). Osteoclasts are formed from the fusion of monocytes/macrophages and are characterized by their large size, the presence of multiple nuclei, and positive staining for tartrate-resistant acid phosphatase (TRAP). Two cytokines, macrophage colony-stimulating factor (M-CSF) and receptor activator of nuclear factor-κB ligand (RANKL), are necessary for the survival and differentiation of macrophages into osteoclasts *in vitro* and *in vivo* (5). The osteoclast attaches to bone via the αvβ3 integrin through formation of the cytoskeletal organizations called actin rings. The resorbing osteoclast has a ruffled membrane and expresses cathepsin K, which is necessary for degrading the organic matrix of bone, and vacuolar proton pumps (H^+-ATPases), which secrete acid and thus result in bone resorption by dissolving the inorganic matrix (5).

The presence of tumor cells in the bone microenvironment results in osteoclast and osteoblast recruitment and activation. This activation stimulates the release of growth factors from stromal cells as well as from the bone matrix, which further promote tumor growth in bone (1–4,6). This is known as the vicious cycle of bone metastasis. We have previously shown that hyperfunctional osteoclasts are permissive for the growth of tumor cells that home to bone (7,8). In addition, mice globally deficient in the β3 integrin, which show a profound defect in platelet and osteoclast function, are protected from bone metastasis and tumor-associated bone destruction (9–11).

CD47 (also called integrin-associated protein) was first isolated through its interaction with the αvβ3 integrin, which is prominently expressed on osteoclasts (12–15). Expressed on all vascular cells, CD47 is an atypical member of the immunoglobulin superfamily (16) with a single IgV domain, five transmembrane segments, and a cytoplasmic tail (17). CD47 associates *in cis* in the plane of the membrane with αvβ3 and other integrins (12–15) and can augment integrin function by this association (18). It has recently been discovered that CD47, when ligated by thrombospondin-1 (TSP1), inhibits nitric oxide (NO) signaling in vascular cells (19). In platelets, TSP1-CD47 signaling opposes the NO/cyclic guanosine 3′,5′-monophosphate (cGMP) inhibition of integrin activation (20), thus facilitating platelet aggregation. CD47 inhibition of NO signaling has also been shown in several other *in vivo* models, suggesting that limiting NO signaling is a primary function of the TSP1-CD47 system (19–26). Recent data indicate that the differentiation of bone marrow macrophages into osteoclast *in vitro* is sensitive to NO concentration, such that low levels of NO stimulate osteoclast formation, whereas increased NO inhibits formation of osteoclast (27). Therefore, CD47 may modulate NO signaling in osteoclast.

Although CD47 associates with αvβ3 and augments its function, $\beta3^{-/-}$ $CD47^{-/-}$ mice have rather different phenotypes. $\beta3^{-/-}$ mice are a model of Glanzmann's thrombasthenia, displaying profound defects in platelet aggregation and clot retraction (10). In contrast, $CD47^{-/-}$ mice have normal bleeding times and a modest decrease in platelet numbers (28). These differences can be accounted by the fact that CD47 augments integrin signaling but is not essential for integrin-mediated adhesion (19). CD47 also has integrin-independent functions. For example, CD47-SIRP1α interactions are important in innate immune reactions, negatively regulating phagocytosis *in vivo*. The presence of CD47 on hematopoietic cells provides them with a "self-signal" that inhibits their phagocytosis (16,29). The SIRP1α-CD47 interaction has also been postulated to be necessary for macrophage fusion, which is essential for the formation of osteoclasts (30,31). Recently, Lundberg and colleagues (31) reported a defect in formation of osteoclasts from macrophages in the presence of blocking antibodies to CD47.

Because CD47 is proposed to function in macrophage fusion, interacts with and activates αvβ3, and modulates NO signaling, we hypothesized that $CD47^{-/-}$ mice would have altered osteoclast differentiation and function. Here, we show that $CD47^{-/-}$ mice have a modest

increase in bone volume due to defective osteoclast function *in vivo*. Furthermore, $CD47^{-/-}$ macrophages are defective in osteoclast formation *in vitro*. The osteoclast defect is rescued by increased administration of RANKL both *in vitro* and *in vivo*, and inhibition of NO synthase (NOS) rescues $CD47^{-/-}$ osteoclast differentiation *in vitro*. To test the role of CD47 in a pathophysiologic context in which osteoclast function is central to disease pathogenesis, we evaluated bone metastasis and tumor-associated bone destruction in $CD47^{-/-}$ mice.

Materials and Methods

Cells

The B16-F10 C57BL/6 murine melanoma cell line was purchased from the American Type Culture Collection and modified to express firefly luciferase (B16-FL; ref. 32).

Animals

$CD47^{-/-}$ mice on a pure C57BL/6 background were housed under pathogen-free conditions according to the guidelines of the Division of Comparative Medicine, Washington University School of Medicine. The animal ethics committee approved all experiments. For generation of $CD47^{-/-}$ mice, $CD47^{+/-}$ females were crossed to $CD47^{+/-}$ males and the females were allowed to have two litters.

Micro–computed tomography

Tibias and femurs were suspended in agarose and the right proximal tibial and femoral metaphyses were scanned by micro–computed tomography (μCT; μCT-40; Scanco Medical) as described previously (33,34). For image acquisition, the tibias were placed in a 17-mm holder and scanned. The image consisted of 50 slices. The trabecular region was selected using contours inside the cortical shell on each two-dimensional image. The growth plate was used as a marker to determine a consistent location to start analysis. A three-dimensional cubical voxel model of bone was built, and the calculations were made as follows: relative bone volume over total bone volume (BV/TV), trabecular number, and thickness. A threshold of 300 (of 1,000) was used to differentiate trabecular bone from nonbone.

Histology, bone histomorphometry, and longitudinal growth measurements

Mouse tibias were fixed in formalin and decalcified in 14% EDTA. Paraffin-embedded sections were stained with H&E and separately for TRAP. Trabecular bone volume and tumor area were measured according to a standard protocol using Bioquant Osteo (Bioquant Image Analysis Corp.). Bone sections were blinded before analysis. Methylmethacrylate-embedded lumbar vertebral bodies of wild-type (WT) and $CD47^{-/-}$ mice were stained for von Kossa on a counterstain of 0.5% basic fuchsin. Longitudinal growth was measured by use of calipers on whole body as well as isolated femurs.

Serum CTX assay

CTX was measured from WT or $CD47^{-/-}$ mouse fasting serum by using a CTX ELISA system (Nordic Bioscience Diagnostics).

Flow cytometry (fluorescence-activated cell sorting)

Whole bone marrow was isolated from WT and $CD47^{-/-}$ mice and incubated in blocking medium (2.4G2 hybridoma with 4 mL of mouse IgG) and then incubated with FITC-conjugated anti-mouse F4/80 or anti-mouse CD47 (miap301) with an anti-rat FITC secondary antibody on ice for 20 min. The cells were then washed twice and analyzed on a FACScan flow cytometer (BD Biosciences).

In vitro osteoclast assays

Whole bone marrow was isolated from WT C57BL/6 mice and plated in M-CSF containing CMG-14–12 cell culture supernatant (1:10, v/v) in α-MEM containing 10% fetal bovine serum in Petri dishes for 3 d to generate primary bone marrow macrophages. Bone marrow macrophages were lifted and equal numbers were plated in 48-well dishes in osteoclast medium, α-MEM containing 10% FBS, CMG-14–12 supernatant (1:20, v/v), and glutathione *S*-transferase–RANKL (50 or 100 ng/mL), and incubated at 37°C for 5 d to generate osteoclasts. TRAP staining was performed according to the manufacturer's instructions (Sigma-Aldrich). In Fig. 4, 0, 3, 10, 30, and 100 μg/mL of *N*-nitro-L-arginine methyl ester (L-NAME) were added to cultures at the same time with M-CSF and RANKL, and medium was changed every day. Osteoclast cultures were fixed after 4 d in culture and stained for TRAP.

Reverse transcription and quantitative PCR

Reverse transcription and quantitative PCR (qPCR) methods were carried out as described previously (8). The following qPCR primers were used: CD47, GGCGCAAAG-CACCGAAGAAATGTT (forward) and CCATGGCATCGCGCTTATCCATTT (reverse); inducible NOS (iNOS), GGCAGCCTGTGAGACCTTTG (forward) and GCATTGGAAGTGAAGCGTTTC (reverse); and glyceraldehyde-3-phosphate dehydrogenase, TCAACAGCAACTCCCACTCTTCCA (forward) and ACCCTGTTGCTGTAGCCGTATTCA (reverse).

Actin ring formation and bone resorption assays

Actin ring formation and bone resorption assays were performed as described (35). Briefly, the cells plated on bovine bone slices were fixed with 3% paraformaldehyde in PBS for 20 min. Filamentous actin was stained with FITC-labeled phalloidin at 0.3 μg/mL in PBS. For staining of the resorption lacunae (pits), the cells were brushed off the bone with a toothbrush. The slices were incubated with 20 μg/mL of peroxidase-conjugated wheat germ agglutinin for 1 h. After washing in PBS, 0.52 mg/mL of 3,3′-diaminobenzidine with 0.1% H_2O_2 was added onto the bone slices for 15 min. Pit area was determined from five ×4 fields by using Osteo software (Bioquant) blinded to genotype.

In vivo RANKL injections

RANKL (100 μg) in a volume of 40 μL was injected subperiostally in the midline calvaria in 8-wk-old mice daily for 5 consecutive days. On the 6th day, serum was collected, mice were sacrificed, and the calvarial bone was isolated. TRAP staining was performed on fixed, decalcified, and paraffin-embedded calvarial bone.

Tumor and bone metastasis models

For intracardiac injections, the operator was blinded to genotype. Mice were anesthetized and inoculated intracardially via the left ventricular chamber with 10^5 B16-FL cells in 50 μL PBS as previously described (7). Bioluminescence imaging was performed on days 7, 10, and 12 after B16-FL cell inoculation. Mice were sacrificed and underwent blinded necropsy on day 12 after tumor cell injection. Mice were discarded from the final analysis if the animal died before day 12 or if necropsy showed a large mediastinal tumor indicative of injection of tumor cells into the chest cavity, not the left ventricle.

For intratibial injections, mice were anesthetized, and 1×10^4 B16-FL cells in 50 μL PBS were injected into the right tibia. PBS (50 μL) was injected into the left tibia as an internal control. Animals were radiographed in two dimensions using an X-ray system to confirm intratibial placement of the needle (Faxitron Corp.). Bioluminescence imaging was performed on days 7 and 9 after B16-FL cell inoculation. Mice were sacrificed and underwent necropsy on day 9

after B16-FL inoculation. Mice with i.m. locations of tumors were discarded from the analysis. For s.c. injections, mice were anesthetized, and 5×10^5 B16-FL cells in 100 μL PBS were injected s.c. on the dorsal surface of the mouse at two sites. Tumor growth was monitored over the 14-d period after B16-FL injections, and bioluminescence imaging was performed 5, 7, 10, and 14 d after B16-FL inoculation. The experiment was terminated due to the presence of large necrotic tumors.

In vivo bioluminescence imaging

Mice were injected i.p. with 150 mg/kg D-luciferin (Biosynthesis) in PBS 10 min before imaging. Imaging was performed using a charge-coupled device camera (IVIS 100; exposure time of 1 or 5 min, binning of 8, field of view of 15 cm, f/stop of 1, and no filter) in collaboration with the Molecular Imaging Center Reporter Core. Mice were anesthetized by isoflurane (2% vaporized in O_2), and C57BL/6 mice were shaved to minimize attenuation of light by pigmented hair. For analysis, total photon flux (photons per second) was measured from a fixed region of interest in the tibia/femur, the mandible, or the local s.c. tumor using Living Image 2.50 and IgorPro software (Wavemetrics).

Results

CD47$^{-/-}$ mice have increased bone volume due to dysfunctional osteoclasts

CD47 interacts with and activates β3 integrins. β3$^{-/-}$ mice display osteopetrosis due to osteoclast dysfunction. Therefore, we hypothesized that CD47$^{-/-}$ mice might have an osteoclast defect. To test this hypothesis, μCT analysis on tibias from 8-week-old WT and CD47$^{-/-}$ littermates was performed. We observed an increase in trabecular BV/TV in CD47$^{-/-}$ mice compared with WT mice (Fig. 1*A* and *B*). There was no change in trabecular number, but the trabecular thickness was increased in CD47$^{-/-}$ tibias (Fig. 1*A* and *B*). Von Kossa staining of the lumbar vertebral bodies, a marker for mineralized matrix, confirmed an increase in bone volume and trabecular thickness in CD47$^{-/-}$ mice (Fig. 1*B*). The increase in trabecular bone volume (BV/TV) was also confirmed by histomorphometry on histologic sections (Fig. 1*C*, *a* and *b*). We did not observe a difference in longitudinal growth of CD47$^{-/-}$ mice as measured by femur length and whole body length (Supplementary Fig. S1). Interestingly, we also observed that osteoclast perimeter/total trabecular bone perimeter was not changed in CD47$^{-/-}$ mice *in vivo* (Fig. 1*C*, *c*). To confirm that this increase in BV/TV was due to dysfunctional osteoclasts, we measured serum CTX, the COOH-terminal telopeptide of collagen type I that is cleaved on bone resorption by osteoclasts. We observed a decrease in CTX activity (Fig. 1*D*), which along with an increase in trabecular bone volume suggests that the osteoclast activity was decreased in CD47$^{-/-}$ mice *in vivo* (Fig. 1*E*).

CD47$^{-/-}$ osteoclast defect can be rescued by high doses of RANKL *in vitro*

To investigate if the osteoclast defect is cell autonomous in CD47$^{-/-}$ mice, we first determined if macrophages or osteoclast precursors were decreased in CD47$^{-/-}$ bone marrow. We stained WT and CD47$^{-/-}$ whole bone marrow with CD47-FITC as control and F4/80 as a macrophage marker and carried out flow cytometry. We did not observe a significant difference in F4/80$^+$ cells in CD47$^{-/-}$ bone marrow compared with WT controls (Fig. 2*A*). To test the differentiation of macrophages to osteoclasts, we cultured whole bone marrow in M-CSF alone for 3 days to enrich for macrophages. An equal number of macrophages were then cultured in the presence of M-CSF and RANKL to promote differentiation into osteoclasts for 7 days. At a dose of 50 ng/mL of RANKL, we observed induction of CD47 transcript levels over the course of osteoclast differentiation in WT but not in CD47$^{-/-}$ cells (Fig. 2*B*). We observed that WT macrophages produced large, multinucleated, TRAP-positive osteoclasts by day 5, but only a few osteoclasts formed from CD47$^{-/-}$ macrophages. When WT and CD47$^{-/-}$ macrophages were plated onto bovine bone slices, there was a decrease in the number of

multinucleated CD47$^{-/-}$ osteoclasts with multiple actin rings visualized by phalloidin staining (Fig. 2*C*). However, when the dose of RANKL was increased 2-fold to 100 ng/mL, the osteoclast differentiation defect was largely rescued in CD47$^{-/-}$ cells. This was reflected in equivalent numbers of osteoclasts with multiple actin rings formed on bovine bone from macrophages of both genotypes (Fig. 2*C*). To determine the functional capacity of CD47$^{-/-}$ osteoclasts to resorb bone, we stained the bones with wheat germ agglutinin to measure the areas of resorption lacunae after 5 days on bovine bone. There was a significant decrease in bone resorption by CD47$^{-/-}$ osteoclasts in 50 ng/mL RANKL; however, the resorption capacity of CD47$^{-/-}$ osteoclasts was similar to WT at a high dose of RANKL (Fig. 2*D*).

The osteoclast dysfunction in CD47$^{-/-}$ mice was rescued by *in vivo* RANKL injections

To determine if RANKL could rescue CD47$^{-/-}$ osteoclast function *in vivo* as was observed *in vitro*, we injected 100 μg RANKL subperiostally into the midline calvaria of 8-week-old WT and CD47$^{-/-}$ mice. We measured serum CTX before and after RANKL injections in these mice. Before RANKL injection, CD47$^{-/-}$ mice had lower serum CTX as we have shown before (Fig. 3*A*). However, after RANKL administration, osteoclast activation was not significantly different between WT and CD47$^{-/-}$ mice as measured by serum CTX (Fig. 3*A*). Furthermore, direct visualization of osteoclast recruitment by TRAP staining on histologic sections of calvarial bone in WT and CD47$^{-/-}$ mice confirmed the CTX results (Fig. 3*B*). We conclude that a high dose of RANKL rescued the cell-autonomous osteoclast defect in CD47$^{-/-}$ mice.

NOS inhibition restores osteoclast differentiation in CD47$^{-/-}$ cells

Several tissues from CD47$^{-/-}$ mice have increased NO levels (36). We differentiated WT and CD47$^{-/-}$ macrophages into osteoclasts in the presence of M-CSF and RANKL. We observed that iNOS expression levels were higher in CD47$^{-/-}$ osteoclast cultures compared with WT controls (Fig. 4*A*). It has been previously shown that increased levels of NO lead to a block in osteoclast differentiation (27). We hypothesized that this increase in NO levels is responsible for the inhibition of osteoclast differentiation in CD47$^{-/-}$ cells. We differentiated WT and CD47$^{-/-}$ macrophages into osteoclasts in the presence of L-NAME, a pan-NOS inhibitor. In CD47$^{-/-}$ cells, we observed a dose-dependent rescue of osteoclast differentiation with L-NAME administration. We observed a biphasic effect of L-NAME on WT cells, where, at a low dose of L-NAME, there was modest enhancement of osteoclast formation and, at a high dose of L-NAME, there was inhibition of osteoclast differentiation (Fig. 4*B*). The osteoclast inhibitory dose of L-NAME on WT cells was enhancing in CD47$^{-/-}$ cells. Taken together, these data support that the increased levels of iNOS in CD47$^{-/-}$ cells negatively affect osteoclast formation.

CD47$^{-/-}$ mice have decreased tumor burden and bone loss in an intracardiac metastasis model

The data above indicate that, at high doses of RANKL, CD47 was not necessary for osteoclast differentiation and function. RANKL is produced from T cells and osteoblasts during inflammatory conditions such as arthritis and bone metastasis. RANKL is not expressed by B16-FL cells (data not shown). We thus examined bone metastasis and osteolysis in CD47$^{-/-}$ mice to determine if this local increase in RANKL is able to rescue the CD47$^{-/-}$ osteoclasts in this pathophysiologic context. We evaluated bone metastasis in WT and CD47$^{-/-}$ mice using murine melanoma B16-F10 cells engineered to express firefly luciferase (B16-FL). We measured bone tumor burden by real-time bioluminescence on days 7, 10, and 12 after intracardiac B16-FL injection, a route of administration that allows for bone metastasis rather than lung infiltration of injected cells (9,32). There was a significant decrease in tumor burden in the femoral/tibial bones and the mandible of CD47$^{-/-}$ mice compared with WT mice (Fig. 5*B* and *C*) as measured by bioluminescence and confirmed by histomorphometric

measurement of tumor volume in histologic sections at day 12 after B16-FL inoculation (Supplementary Fig. S2*A*;Fig. 5*B* and *C*). Tumor cells are known to secrete factors that activate osteoclasts to degrade bone and induce osteolysis, which is a significant outcome of bone metastases (1–4,6). Trabecular bone volume was measured in WT and CD47$^{-/-}$ mice injected with B16-FL or saline. Whereas there was significant bone loss in B16-FL in WT mice, there was no bone loss in CD47$^{-/-}$ bones injected with B16-FL, consistent with the osteoclast dysfunction in CD47$^{-/-}$ mice (Fig. 5*B* and *C*). We did not observe a difference in osteoclast perimeter/trabecular bone perimeter in tumor-bearing CD47$^{-/-}$ bones (Fig. 5*D*). Thus, we conclude that CD47$^{-/-}$ mice had decreased bone tumor burden and tumor-associated bone destruction, and the local increase in RANKL levels *in vivo* was not sufficient to rescue the osteoclast defect in CD47$^{-/-}$ mice.

CD47$^{-/-}$ mice have decreased tumor burden and bone loss in an intratibial metastasis model but not in a s.c. model

We have previously shown that platelets are critical for the homing of tumor cells to bone (9). CD47$^{-/-}$ mice have been shown to have a mild decrease in platelet numbers (28). To further confirm that this decrease in tumor burden in CD47$^{-/-}$ mice after intracardiac injections of B16-FL cells was not due to compromised homing of tumor cells to bone, we turned to a more direct model of late-stage bone metastasis that eliminates initial tumor-homing steps of the metastatic process. We injected equal numbers of B16-FL cells directly into the tibiae of WT and CD47$^{-/-}$ littermates and performed bioluminescence on days 7 and 9 after B16-FL inoculation. Bioluminescence imaging showed decreased tumor burden over time in the CD47$^{-/-}$ mice compared with WT mice (Fig. 6*A*). Histomorphometric measurement of tumor volume in histologic sections at day 9 after B16-FL inoculation confirmed this decrease (Supplementary Fig. S2*B*; Fig. 6*B*).

To confirm that the decrease in bone tumor burden in CD47$^{-/-}$ mice was specific to CD47 function in the bone microenvironment and not a result of intervention by the immune system or tumor-associated angiogenesis in the CD47$^{-/-}$ mice, we measured local tumor burden in s.c. injected B16-FL cells. We observed no change in s.c. tumor burden as measured by bioluminescence on days 5, 7, 10, and 14, at which point the experiment was terminated due to necrotic tumors (Fig. 6*C*). We conclude that the decrease in tumor burden in CD47$^{-/-}$ mice was specific to the bone compartment and not due to compromised immunity or platelet interactions.

Discussion

We show here that CD47$^{-/-}$ mice exhibited mild osteopetrosis and decreased osteoclast function *in vivo* and *in vitro*. *In vitro*, CD47$^{-/-}$ macrophages did not form as many multinucleated spread osteoclasts as WT cells. Bone resorption as measured by pit staining was decreased in CD47$^{-/-}$ cells *in vitro*. Interestingly, this osteoclast defect was rescued by delivery of high doses of RANKL both *in vitro* and *in vivo*, suggesting that CD47 may cooperate with RANKL during osteoclast development/function. We observed that iNOS levels were increased in CD47$^{-/-}$ osteoclasts and inhibition of NOS rescued the osteoclast differentiation defect in CD47$^{-/-}$ cells. We also observed decreased tumor burden and osteolysis in CD47$^{-/-}$ bone after intracardiac or intratibial delivery of tumor cells.

The first role known for CD47 was based on its physical and functional interaction with αvβ3 (37). It is well known that the integrin αvβ3 plays a critical role not only in osteoclast function (11) but also in the differentiation of macrophages into osteoclast (38). CD47 has been shown to augment αvβ3 function by physical association, leading to increased integrin clustering and therefore increases in avidity. Furthermore, CD47 signals through Gai to activate αvβ3 via an “inside-out” signaling pathway analogous to that used by G protein–coupled receptors on

platelets to activate αIIbβ3 via activation of the small G protein Rap1 (20). In platelets, NO-stimulated cGMP levels oppose Rap1b activation. CD47 acts to prevent this inhibitory effect of NO, thus allowing more GTP loading of Rap1b, resulting in αIIbβ3 activation (20). It is likely that CD47 in osteoclasts can activate αvβ3 in a similar fashion.

Although CD47 could be playing a role in osteoclast differentiation and function by augmenting αvβ3 signaling, it could also exert its effects on osteoclasts in a β3-independent manner. The defect in osteoclast differentiation can be overcome by addition of high doses of M-CSF to cultures by increasing expression of c-fms (39). In contrast, we observed that exogenous RANKL administration could rescue the osteoclast defect in CD47$^{-/-}$ mice *in vivo* and *in vitro*, suggesting that CD47 might play a role in osteoclastogenesis by enhancing RANKL signaling. It is possible that CD47 and RANKL might stimulate osteoclasts in parallel pathways that merge at a common signaling molecule. Our data suggest that the NO/cGMP pathway might be the link between CD47 and RANKL signaling.

There is a growing literature on the role of NO in osteoclast differentiation and function. Often, the proposed “Goldilocks effect” comes into play in NO regulation. NO has been reported to both promote and inhibit osteoclast differentiation/survival (27,40,41) and osteoclast function (40,42,43). Low signaling levels of NO derived from eNOS (NOSIII) and/or nNOS (NOSI) are most likely needed to support osteoclast differentiation, whereas higher levels, such as those produced by iNOS, become inhibitory. We found that iNOS was significantly induced in CD47$^{-/-}$ osteoclast and inhibition with a NOS inhibitor, L-NAME, rescued CD47$^{-/-}$ osteoclast differentiation (Fig. 4*B*). Many signaling effects of NO are mediated via stimulation of soluble guanylate cyclase, production of cGMP, and activation of protein kinase G. However, there are effects of NO that are accomplished by its direct interaction with protein thiols (*S*-nitrosylation) to modify their enzymatic activity (44,45). Src, a kinase downstream of RANK signaling known to have a critical role in osteoclast differentiation and function (46), is a target of inhibitory *S*-nitrosylation (47). This modification of Src by NO in osteoclasts might have a significant effect on osteoclast function. Such a finely balanced regulatory mechanism is suggested by our finding that only a 2-fold increase in RANKL concentration *in vitro* permits formation of CD47$^{-/-}$ osteoclasts that are as functional as WT osteoclasts.

The second major finding of our study is that the role of CD47 in osteoclast differentiation/function has a significant effect on the interaction of tumor cells within the bone microenvironment. The decreased osteoclast function in CD47$^{-/-}$ mice leads to a decrease in bone tumor burden and osteolysis, consistent with the model of the vicious cycle of bone metastasis (1–4). Notably, the increase in bone volume in CD47$^{-/-}$ was only ~4% compared with WT mice, not as profound a change as observed in the osteopetrotic β3$^{-/-}$ mice (11). It is interesting that the relatively modest, rescuable decrease in osteoclast function in CD47$^{-/-}$ mice *in vivo* could result in a more pronounced decrease in tumor burden and osteolysis. These results suggest that the relationship between the osteoclast and the tumor cell with regard to the vicious cycle of bone metastasis is not one of direct proportionality. The complex signaling pathways involved in the relationship between tumor cells and bone cells no doubt involve amplification steps. Both Src kinase–initiated pathways and the NO/cGMP pathways implicated here are classic examples of signal amplifiers.

One of the major complications of currently available therapies for bone metastasis, such as bisphosphonates, is their harsh effect on bone, leading to conditions such as suppressed bone turnover or osteonecrosis of the jaw (48,49). We observed that CD47$^{-/-}$ mice displayed a mild increase in bone volume and a decrease in tumor burden in bone. Our results suggest the potential for manipulating CD47 signaling as a novel approach to treatment of osteoporosis in the general population and to treatment of bone metastasis in cancer patients without causing severe complications to the skeleton.

Supplementary Material

Refer to Web version on PubMed Central for supplementary material.

Acknowledgments

Grant support: Cancer Biology Pathway, Kauffman Fellowship, St. Louis Men's Group Against Cancer, Washington University Molecular Imaging Center grant P50 CA94056, NIH grant HL54390 (W.A. Frazier), and NIH grant R01-CA097250 (K.N. Weilbaecher, Ö. Uluçkan, S.N. Becker, H. Deng).

We thank Dr. F. Patrick Ross, Dr. Deborah Novack, Dr. Steven Teitelbaum, Dr. Roberta Faccio, Dr. Desiree H. Floyd, Dr. Elizabeth A. Morgan, Angela Hirbe, Valerie Salazar, and Carlos I. Michel for helpful discussions; Crystal Idleburg for expert animal histology; and Lei Zhao for animal husbandry.

References

1. Mundy GR. Metastasis to bone: causes, consequences and therapeutic opportunities. Nat Rev Cancer 2002;2:584–593. [PubMed: 12154351]
2. Kingsley LA, Fournier PG, Chirgwin JM, Guise TA. Molecular biology of bone metastasis. Mol Cancer Ther 2007;6:2609–2617. [PubMed: 17938257]
3. Kozlow W, Guise TA. Breast cancer metastasis to bone: mechanisms of osteolysis and implications for therapy. J Mammary Gland Biol Neoplasia 2005;10:169–180. [PubMed: 16025223]
4. Roodman GD. Mechanisms of bone metastasis. N Engl J Med 2004;350:1655–1664. [PubMed: 15084698]
5. Teitelbaum SL, Ross FP. Genetic regulation of osteoclast development and function. Nat Rev Genet 2003;4:638–649. [PubMed: 12897775]
6. Clines GA, Guise TA. Molecular mechanisms and treatment of bone metastasis. Expert Rev Mol Med 2008;10:e7. [PubMed: 18321396]
7. Hirbe AC, Uluckan O, Morgan EA, et al. Granulocyte colony-stimulating factor enhances bone tumor growth in mice in an osteoclast-dependent manner. Blood 2007;109:3424–3431. [PubMed: 17192391]
8. Hirbe AC, Rubin J, Uluckan O, et al. Disruption of CXCR4 enhances osteoclastogenesis and tumor growth in bone. Proc Natl Acad Sci U S A 2007;104:14062–14067. [PubMed: 17715292]
9. Bakewell SJ, Nestor P, Prasad S, et al. Platelet and osteoclast β3 integrins are critical for bone metastasis. Proc Natl Acad Sci U S A 2003;100:14205–14210. [PubMed: 14612570]
10. Hodivala-Dilke KM, McHugh KP, Tsakiris DA, et al. β3-Integrin-deficient mice are a model for Glanzmann thrombasthenia showing placental defects and reduced survival. J Clin Invest 1999;103:229–238. [PubMed: 9916135]
11. McHugh KP, Hodivala-Dilke K, Zheng MH, et al. Mice lacking β3 integrins are osteosclerotic because of dysfunctional osteoclasts. J Clin Invest 2000;105:433–440. [PubMed: 10683372]
12. Gao AG, Lindberg FP, Dimitry JM, Brown EJ, Frazier WA. Thrombospondin modulates avβ3 function through integrin-associated protein. J Cell Biol 1996;135:533–544. [PubMed: 8896608]
13. Chung J, Gao AG, Frazier WA. Thrombospondin acts via integrin-associated protein to activate the platelet integrin aIIbβ3. J Biol Chem 1997;272:14740–14746. [PubMed: 9169439]
14. Chung J, Wang XQ, Lindberg FP, Frazier WA. Thrombospondin-1 acts via IAP/CD47 to synergize with collagen in a2β1-mediated platelet activation. Blood 1999;94:642–648. [PubMed: 10397731]
15. Wang XQ, Frazier WA. The thrombospondin receptor CD47 (IAP) modulates and associates with a2β1 integrin in vascular smooth muscle cells. Mol Biol Cell 1998;9:865–874. [PubMed: 9529384]
16. Oldenborg PA, Zheleznyak A, Fang YF, Lagenaur CF, Gresham HD, Lindberg FP. Role of CD47 as a marker of self on red blood cells. Science 2000;288:2051–2054. [PubMed: 10856220]
17. Lindberg FP, Gresham HD, Schwarz E, Brown EJ. Molecular cloning of integrin-associated protein: an immunoglobulin family member with multiple membrane-spanning domains implicated in avβ3-dependent ligand binding. J Cell Biol 1993;123:485–496. [PubMed: 7691831]
18. McDonald JF, Zheleznyak A, Frazier WA. Cholesterol-independent interactions with CD47 enhance avβ3 avidity. J Biol Chem 2004;279:17301–17311. [PubMed: 14966135]

19. Isenberg JS, Hyodo F, Pappan LK, et al. Blocking thrombospondin-1/CD47 signaling alleviates deleterious effects of aging on tissue responses to ischemia. Arterioscler Thromb Vasc Biol 2007;27:2582–2588. [PubMed: 17916772]
20. Isenberg JS, Romeo MJ, Yu C, et al. Thrombospondin-1 stimulates platelet aggregation by blocking the antithrombotic activity of nitric oxide/cGMP signaling. Blood 2008;111:613–623. [PubMed: 17890448]
21. Isenberg JS, Annis DS, Pendrak ML, et al. Differential interactions of thrombospondins-1,−2, and −4 with CD47 and effects on cGMP signaling and ischemic injury responses. J Biol Chem 2009;284:1116–1125. [PubMed: 19004835]
22. Isenberg JS, Jia Y, Fukuyama J, Switzer CH, Wink DA, Roberts DD. Thrombospondin-1 inhibits nitric oxide signaling via CD36 by inhibiting myristic acid uptake. J Biol Chem 2007;282:15404–15415. [PubMed: 17416590]
23. Isenberg JS, Maxhimer JB, Hyodo F, et al. Thrombospondin-1 and CD47 limit cell and tissue survival of radiation injury. Am J Pathol 2008;173:1100–1112. [PubMed: 18787106]
24. Isenberg JS, Pappan LK, Romeo MJ, et al. Blockade of thrombospondin-1-CD47 interactions prevents necrosis of full thickness skin grafts. Ann Surg 2008;247:180–190. [PubMed: 18156939]
25. Isenberg JS, Ridnour LA, Dimitry J, Frazier WA, Wink DA, Roberts DD. CD47 is necessary for inhibition of nitric oxide-stimulated vascular cell responses by thrombospondin-1. J Biol Chem 2006;281:26069–26080. [PubMed: 16835222]
26. Isenberg JS, Romeo MJ, Abu-Asab M, et al. Increasing survival of ischemic tissue by targeting CD47. Circ Res 2007;100:712–720. [PubMed: 17293482]
27. Zheng H, Yu X, Collin-Osdoby P, Osdoby P. RANKL stimulates inducible nitric-oxide synthase expression and nitric oxide production in developing osteoclasts. An autocrine negative feedback mechanism triggered by RANKL-induced interferon-β via NF-κB that restrains osteoclastogenesis and bone resorption. J Biol Chem 2006;281:15809–15820. [PubMed: 16613848]
28. Olsson M, Bruhns P, Frazier WA, Ravetch JV, Oldenborg PA. Platelet homeostasis is regulated by platelet expression of CD47 under normal conditions and in passive immune thrombocytopenia. Blood 2005;105:3577–3582. [PubMed: 15665111]
29. Wang H, Madariaga ML, Wang S, Van Rooijen N, Oldenborg PA, Yang YG. Lack of CD47 on nonhematopoietic cells induces split macrophage tolerance to CD47null cells. Proc Natl Acad Sci U S A 2007;104:13744–13749. [PubMed: 17699632]
30. Vignery A. Macrophage fusion: the making of osteoclasts and giant cells. J Exp Med 2005;202:337–340. [PubMed: 16061722]
31. Lundberg P, Koskinen C, Baldock PA, et al. Osteoclast formation is strongly reduced both in vivo and in vitro in the absence of CD47/SIRPα-interaction. Biochem Biophys Res Commun 2007;352:444–448. [PubMed: 17126807]
32. Uluckan O, Eagleton MC, Floyd DH, et al. APT102, a novel adpase, cooperates with aspirin to disrupt bone metastasis in mice. J Cell Biochem 2008;104:1311–1323. [PubMed: 18260128]
33. Lane NE, Yao W, Nakamura MC, et al. Mice lacking the integrin β5 subunit have accelerated osteoclast maturation and increased activity in the estrogen-deficient state. J Bone Miner Res 2005;20:58–66. [PubMed: 15619670]
34. Christiansen BA, Silva MJ. The effect of varying magnitudes of whole-body vibration on several skeletal sites in mice. Ann Biomed Eng 2006;34:1149–1156. [PubMed: 16786394]
35. Zhao H, Laitala-Leinonen T, Parikka V, Vaananen HK. Downregulation of small GTPase Rab7 impairs osteoclast polarization and bone resorption. J Biol Chem 2001;276:39295–39302. [PubMed: 11514537]
36. Isenberg JS, Roberts DD, Frazier WA. CD47: a new target in cardiovascular therapy. Arterioscler Thromb Vasc Biol 2008;28:615–621. [PubMed: 18187671]
37. Brown EJ, Frazier WA. Integrin-associated protein (CD47) and its ligands. Trends Cell Biol 2001;11:130–135. [PubMed: 11306274]
38. Ross FP, Teitelbaum SL. avβ3 and macrophage colony-stimulating factor: partners in osteoclast biology. Immunol Rev 2005;208:88–105. [PubMed: 16313343]
39. Faccio R, Takeshita S, Zallone A, Ross FP, Teitelbaum SL. c-Fms and the avβ3 integrin collaborate during osteoclast differentiation. J Clin Invest 2003;111:749–758. [PubMed: 12618529]

40. Jung JY, Lin AC, Ramos LM, Faddis BT, Chole RA. Nitric oxide synthase I mediates osteoclast activity in vitro and in vivo. J Cell Biochem 2003;89:613–621. [PubMed: 12761894]
41. Lee SK, Huang H, Lee SW, et al. Involvement of iNOS-dependent NO production in the stimulation of osteoclast survival by TNF-α. Exp Cell Res 2004;298:359–368. [PubMed: 15265685]
42. Tan SD, de Vries TJ, Kuijpers-Jagtman AM, Semeins CM, Everts V, Klein-Nulend J. Osteocytes subjected to fluid flow inhibit osteoclast formation and bone resorption. Bone 2007;41:745–751. [PubMed: 17855178]
43. van't Hof RJ, Macphee J, Libouban H, Helfrich MH, Ralston SH. Regulation of bone mass and bone turnover by neuronal nitric oxide synthase. Endocrinology 2004;145:5068–5074. [PubMed: 15297441]
44. Derakhshan B, Hao G, Gross SS. Balancing reactivity against selectivity: the evolution of protein S-nitrosylation as an effector of cell signaling by nitric oxide. Cardiovasc Res 2007;75:210–219. [PubMed: 17524376]
45. Isenberg JS, Frazier WA, Roberts DD. Thrombospondin-1: a physiological regulator of nitric oxide signaling. Cell Mol Life Sci 2008;65:728–742. [PubMed: 18193160]
46. Zou W, Kitaura H, Reeve J, et al. Syk, c-Src, the avβ3 integrin, and ITAM immunoreceptors, in concert, regulate osteoclastic bone resorption. J Cell Biol 2007;176:877–888. [PubMed: 17353363]
47. Akhand AA, Pu M, Senga T, et al. Nitric oxide controls src kinase activity through a sulfhydryl group modification-mediated Tyr-527-independent and Tyr-416-linked mechanism. J Biol Chem 1999;274:25821–25826. [PubMed: 10464322]
48. Armamento-Villareal R, Napoli N, Panwar V, Novack D. Suppressed bone turnover during alendronate therapy for high-turnover osteoporosis. N Engl J Med 2006;355:2048–2050. [PubMed: 17093260]
49. Hirbe A, Morgan EA, Uluckan O, Weilbaecher K. Skeletal complications of breast cancer therapies. Clin Cancer Res 2006;12:6309s–6314s. [PubMed: 17062720]

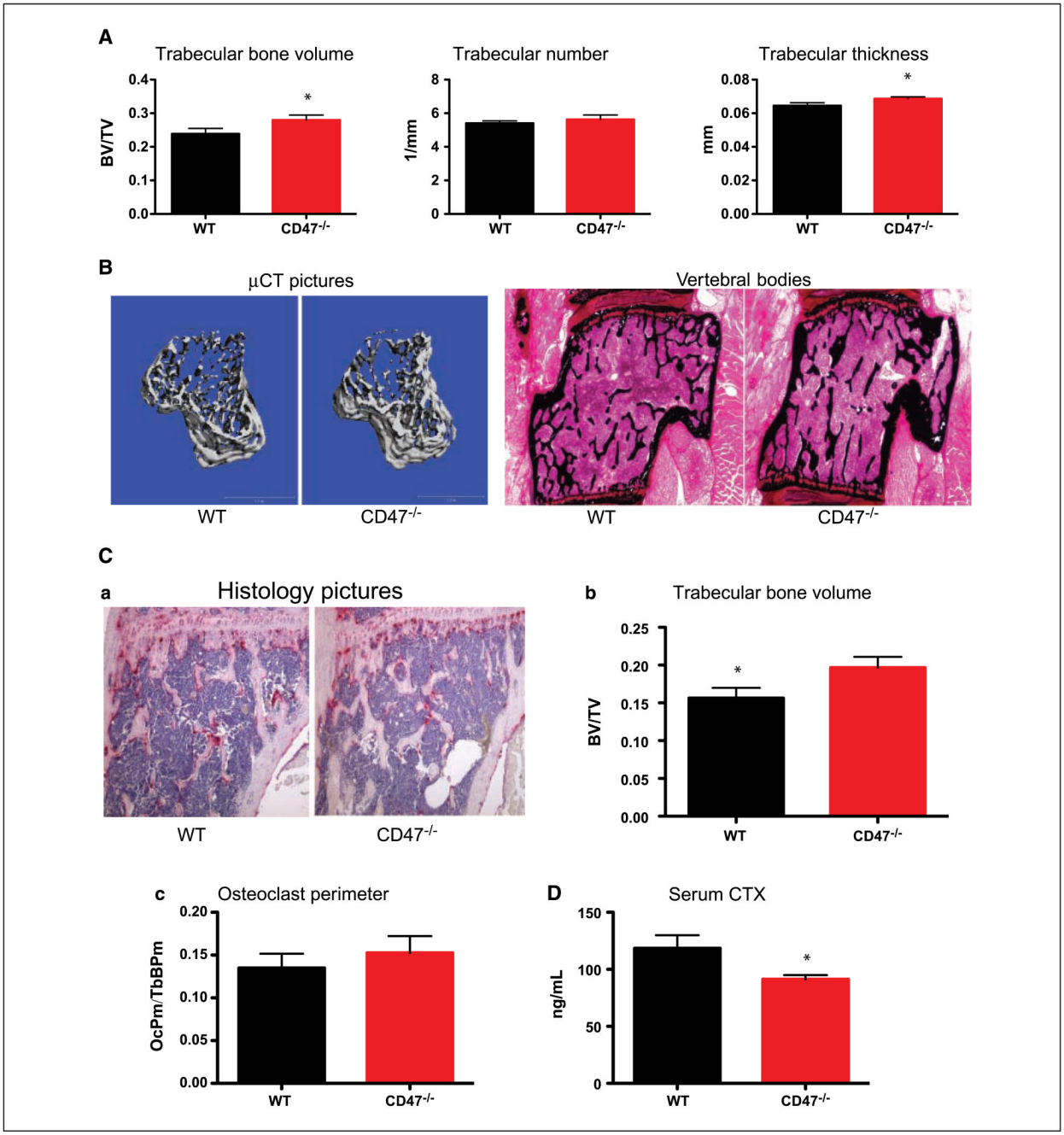

Figure 1.

CD47$^{-/-}$ mice have increased bone volume due to dysfunctional osteoclasts. *A*, WT and CD7$^{-/-}$ tibias were subjected to μCT analysis of bone parameters (WT, $n = 5$; CD47$^{-/-}$, $n = 5$). Trabecular BV/TV by μCT ($P = 0.04$); trabecular number by μCT ($P = 0.22$); trabecular thickness by μCT ($P = 0.04$). *B*, representative images of three-dimensional μCT reconstruction of WT and CD47$^{-/-}$ tibias (*left*) and lumbar vertebral bodies of WT and CD47$^{-/-}$ mice stained with von Kossa (*right*). *C*, *a*, representative histologic TRAP-stained tibial sections. *b*, BV/TV in tibias by histomorphometry ($P = 0.02$). *c*, osteoclast perimeter/trabecular bone perimeter ($P = 0.23$). *D*, collagen breakdown products (CTX) were measured in the serum of starved WT and CD47$^{-/-}$ mice ($P = 0.03$).

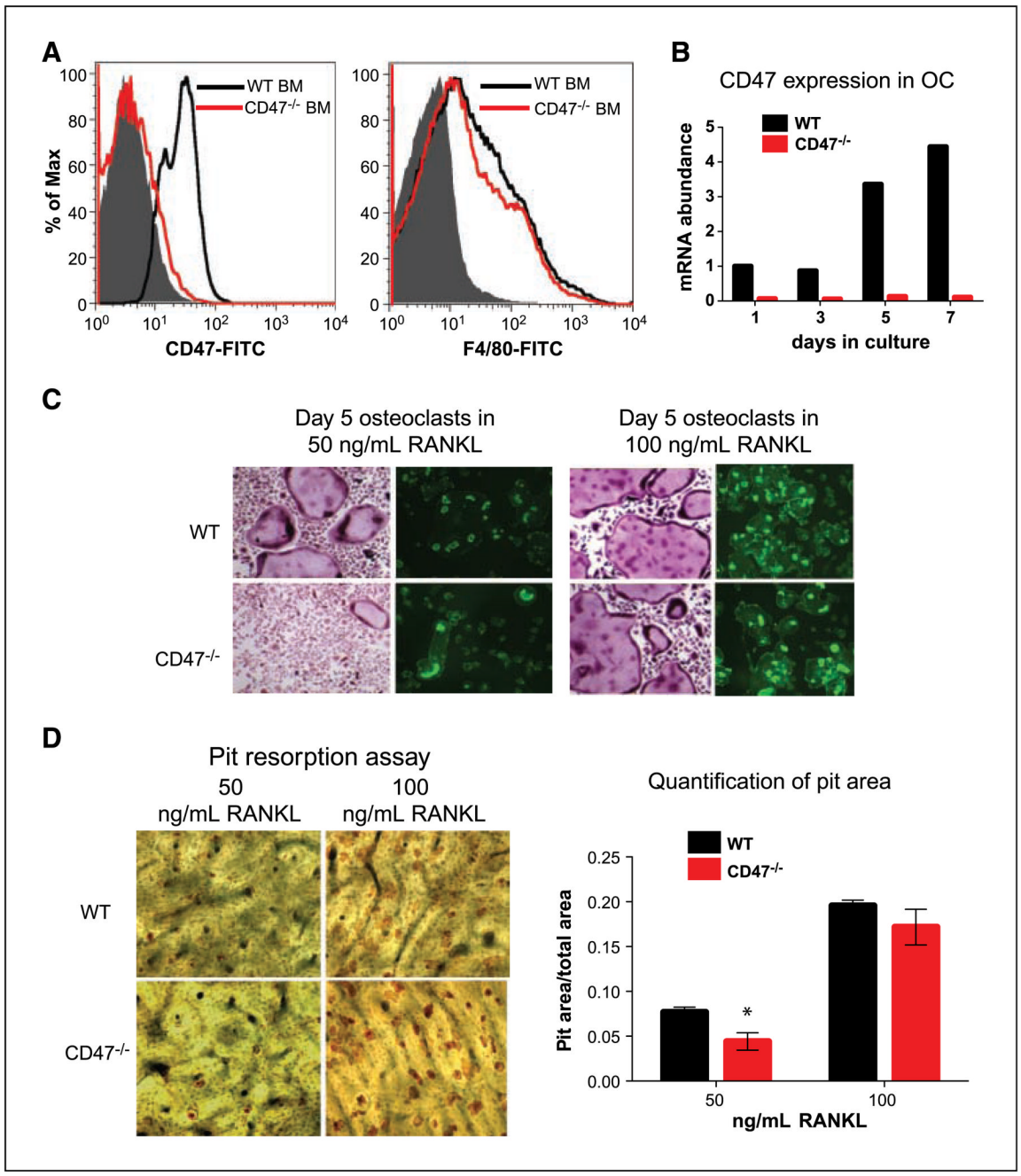

Figure 2.

CD47$^{-/-}$ osteoclast defect can be rescued by high doses of RANKL *in vitro*. *A*, fluorescence-activated cell sorting analysis on WT and CD47$^{-/-}$ total bone marrow (*BM*). WT and CD47$^{-/-}$ total bone marrow was stained for CD47 and F4/80. *B*, qPCR graph showing induction of CD47 transcript over the 7-d course of osteoclast differentiation. *C*, representative images of day 5 osteoclasts cultured on bone and stained for TRAP (*left*) and cultured on bovine bone and stained for actin rings (*right*) in the presence of 50 ng/mL M-CSF and 50 or 100 ng/mL of RANKL. *D*, representative images of day 5 osteoclasts cultured on bone and stained for resorption lacunae in the presence of 50 ng/mL M-CSF and either 50 or 100 ng/mL of RANKL.

The pit (resorption lacunae) area was measured by histomorphometry. RANKL: 50 ng/mL ($P = 0.04$) and 100 ng/mL ($P = 0.18$).

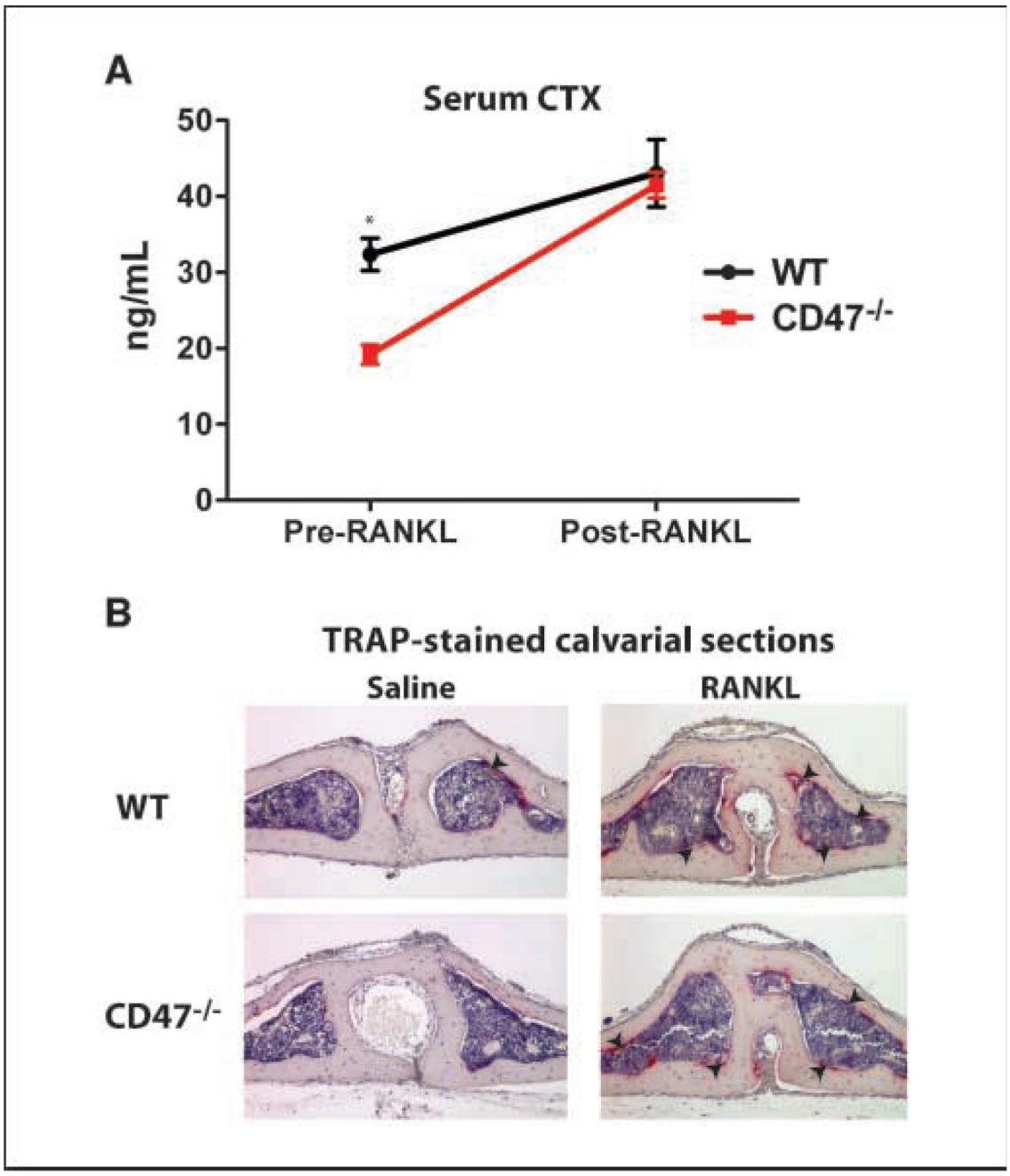

Figure 3.

The osteoclast dysfunction in CD47$^{-/-}$ mice is rescued by *in vivo* RANKL injections. *A*, 100 μg RANKL was delivered subperiostally onto the midline calvaria of WT ($n = 5$) and CD47$^{-/-}$ ($n = 5$) mice. Serum CTX was measured before and after RANKL injections. WT versus CD47$^{-/-}$ pre-RANKL, $P < 0.01$; WT versus CD47$^{-/-}$ post-RANKL, $P = 0.74$; WT pre-RANKL versus post-RANKL, $P = 0.03$; CD47$^{-/-}$ pre-RANKL versus post-RANKL, $P < 0.01$. *B*, representative images of TRAP-stained calvarial sections. *Arrows*, recruited osteoclasts.

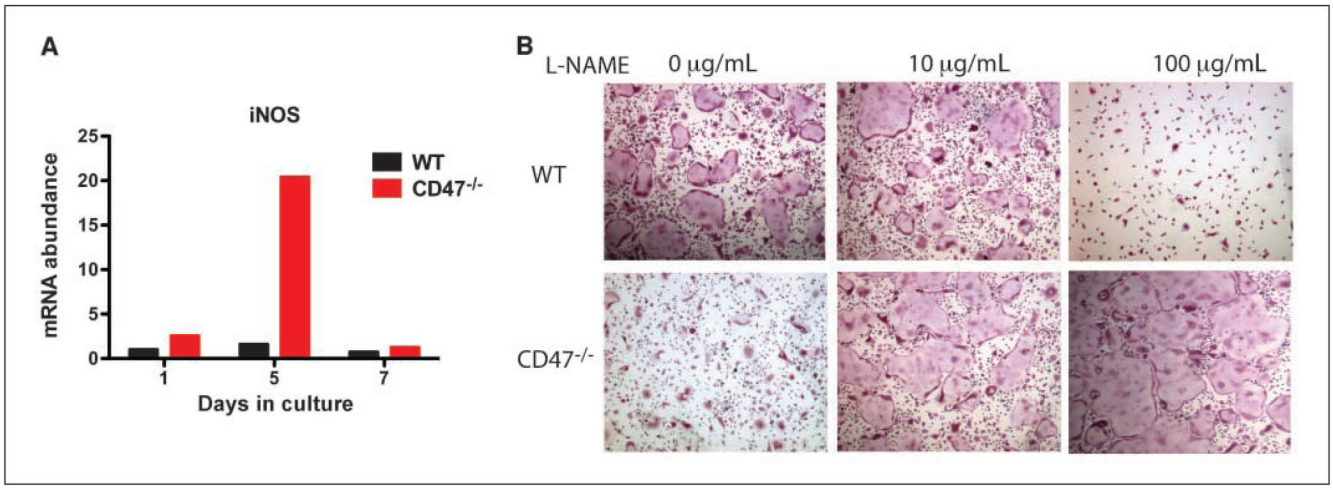

Figure 4.

NOS inhibition restores osteoclast differentiation in CD47$^{-/-}$ cells. *A*, WT and CD47$^{-/-}$ macrophages were differentiated into osteoclast in the presence of 50 ng/mL M-CSF and 50 ng/mL RANKL. RNA was isolated at days 1, 5, and 7, and cDNA was made. qPCR analysis was carried out with specific primers to iNOS. *B*, WT and CD47$^{-/-}$ macrophages were differentiated into osteoclasts in the presence of M-CSF, RANKL, and L-NAME, a pan-inhibitor of NOS, for 5 d.

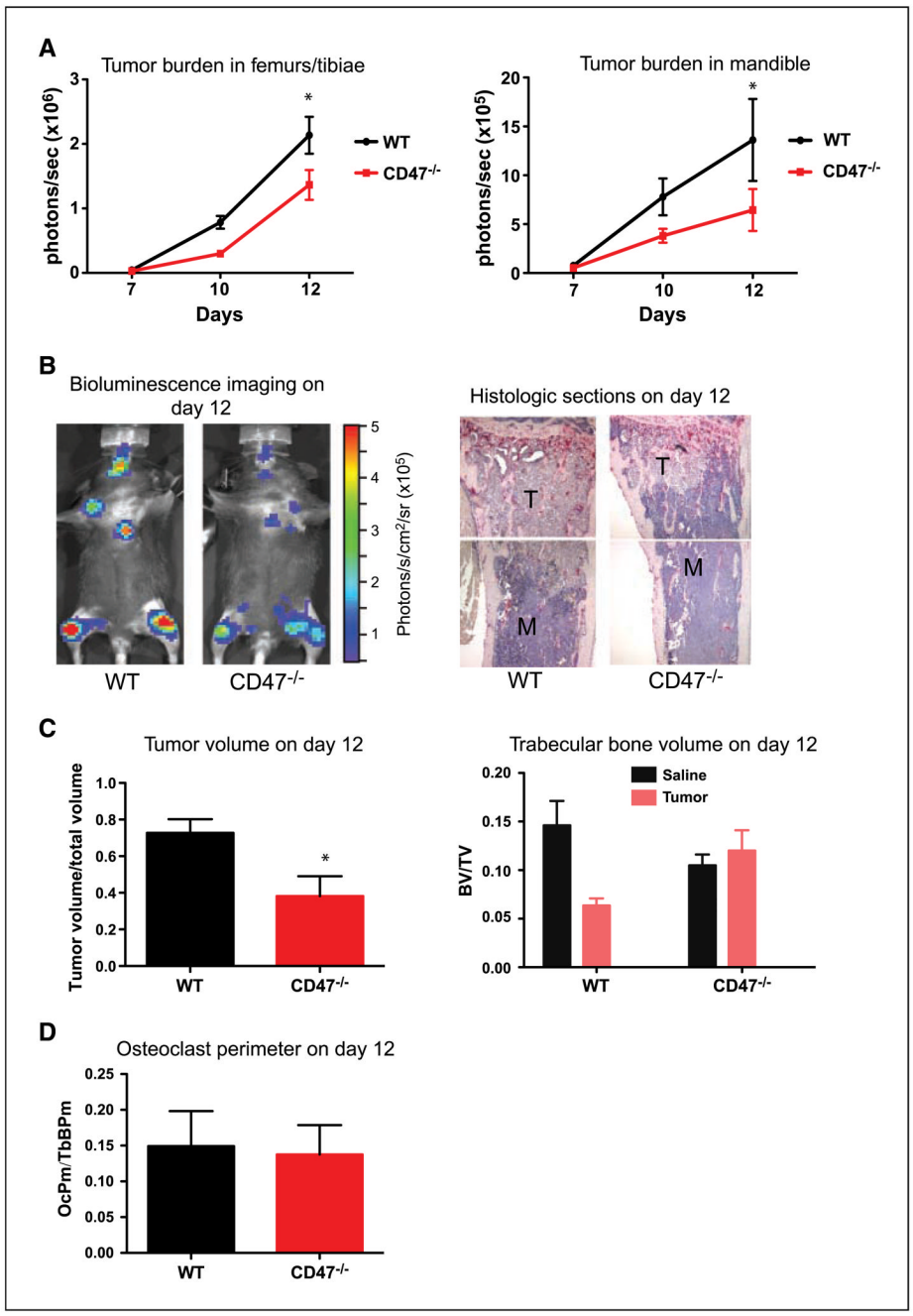

Figure 5.

CD47$^{-/-}$ mice have decreased tumor burden and bone loss in an intracardiac metastasis model. *A*, B16-FL cells were injected into the left ventricular chamber of WT (n = 3) and CD47$^{-/-}$ (n = 3) mice. Tumor burden in the femur/tibia (P = 0.003) and the mandible (P = 0.05) as measured by bioluminescence imaging 7, 10, and 12 d after tumor cell injection. *B*, representative images of bioluminescence and of tibial histologic bone sections. *M*, marrow; *T*, tumor. *C*, tumor volume/total volume in the tibias of WT (n = 3) and CD47$^{-/-}$ (n = 3) mice at day 12 was measured by histomorphometric analysis (P = 0.02). Trabecular bone volume in the tibias of WT (n = 3) and CD47$^{-/-}$ (n = 3) mice at day 12 was measured by histomorphometric analysis. WT saline versus tumor, $P < 0.01$; CD47$^{-/-}$ saline versus tumor,

$P = 0.51$. *D*, osteoclast perimeter in the tibias of WT ($n = 3$) and CD47$^{-/-}$ ($n = 3$) mice at day 12 was measured by histomorphometric analysis. Three independent experiments showed similar results.

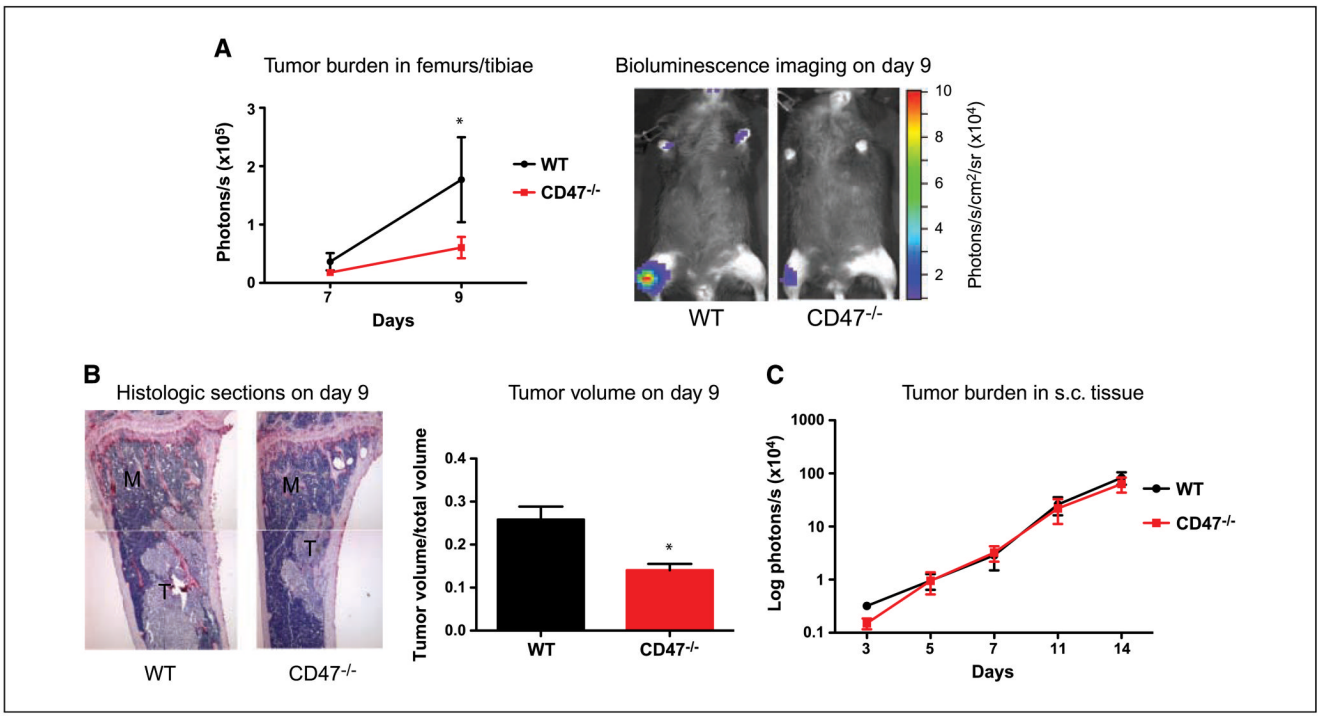

Figure 6.

$CD47^{-/-}$ mice have decreased tumor burden and bone loss in an intratibial metastasis model but not in a s.c. model. *A*, B16-FL cells were injected directly into the tibia of WT ($n = 6$) and $CD47^{-/-}$ ($n = 5$) mice. Tumor burden in the tibiae was measured by bioluminescence imaging at days 7 and 9 after B16-FL injection ($P = 0.05$). Representative bioluminescence images are shown. *B*, representative images of tibial histologic bone sections at day 9. Tumor volume/total volume in the tibias of WT ($n = 6$) and $CD47^{-/-}$ ($n = 5$) mice at day 12 was measured by histomorphometric analysis ($P = 0.03$). Three independent experiments showed similar results. *C*, B16-FL cells were injected s.c. into the hind flank of mice, and tumor burden was measured by bioluminescence imaging at days 5, 7, 10, and 14 after B16-FL injection.